RESEARCH ARTICLE

WILEY

Combination of historical and modern data to decipher the geomorphic evolution of the Innere Ölgruben rock glacier, Kaunertal, Austria, over almost a century (1922–2021)

Fabian Fleischer[1] | Florian Haas[1] | Moritz Altmann[1] | Jakob Rom[1] | Bettina Knoflach[2] | Michael Becht[1]

[1]Department of Physical Geography, Catholic University of Eichstätt-Ingolstadt, Eichstätt, Germany

[2]Department of Geography, University of Innsbruck, Innsbruck, Austria

Correspondence
Fabian Fleischer, Department of Physical Geography, Catholic University of Eichstätt-Ingolstadt, 95072 Eichstätt, Germany.
Email: fabian.fleischer@ku.de

Abstract

Rock glaciers are cryo-conditioned downslope-creeping landforms in high mountains. Their dynamics are changing due to external factors influenced by climate change. Although there has been a growing scientific interest in mountain permafrost and thus in rock glaciers in recent years, their historical development, especially before the first alpine-wide aerial image flights in the 1950s, has hardly been researched. Therefore, we utilize a historical stereophotogrammetric map from 1922 and historical flow velocity profiles (1938–1953) and relate them to data derived from historical aerial photographs and airborne laser scanning data in several time slices between 1953 and 2021. By doing so, the development of flow velocity, surface elevation changes, and frontal advance of the two lobes of the composite rock glacier Inner Ölgrube, Kaunertal, Austria, is analyzed and compared over almost a century. Results indicate an increased frontal advance in the laterally confined area of one lobe and a severe subsidence in the upper area of both lobes between 1922 and 1953. Whereas the former could be explained by a combination of the short warm phase in the 1940s and 1950s and the (subsurface) topography, the latter might be attributed to the strong melting of superimposed debris-covered dead ice bodies, a relict of the Little Ice Age (LIA) glaciation. Both factors might also contribute to the increased flow velocities between 1938 and 1953, which are still recognizable in the 1953–1970 time step. Although both lobes follow a general similar trend, which is in line with the alpine-wide trend of flow velocity acceleration in the 1990s, differences in the geomorphic development of the two lobes were identified. In addition to a slightly varying evolution of the flow velocities, the timing and magnitude of the volume changes are different. Furthermore, both lobes display a dissimilar mechanism of frontal advance over the entire study period. Because the external forcing is identical, the varying development might be attributed to variations in internal structure, bedrock topography, or upslope connection of the lobes. Due to the lateral constriction, the subsurface topography, and the LIA maximum extent of the glacier, it is assumed that

the geomorphic development of the Innere Ölgruben rock glacier, particularly before 1953, represents a special case, and the results are not simply transferable to other rock glaciers.

1 | INTRODUCTION

Active rock glaciers are a downslope creep phenomenon of mountain permafrost that occurs in areas with high-relief and suitable topoclimatic conditions.[1–3] The growing interest of the scientific community in mountain permafrost has led to rapid progress in the understanding of rock glaciers in recent years mainly in the European Alps (e.g., Haeberli et al.,[3] Buchli et al.,[4] Cicoira et al.,[5] Cicoira et al.,[6] Gärtner-Roer et al.,[7] Kellerer-Pirklbauer and Kaufmann,[8] Kenner et al.,[9] Krainer et al.,[10] Kummert et al.,[11] Marcer et al.,[12] and Wagner et al.[13]) but also in other mountain regions such as the Andes (e.g., Rangecroft et al.[14] and Schaffer et al.[15]) or the Himalayas (e.g., Jones et al.[16] and Knight et al.[17]).

Studies on the current inter-, intra-, and multi-annual kinematics of rock glaciers and their forcing factors (e.g., Cicoira et al.,[6] Kenner et al.,[9] Delaloye et al.,[18] Delaloye et al.,[19] Kenner et al.,[20] and Wirz et al.[21]) and studies investigating the long-term kinematic development of rock glaciers over several decades are available. These multi-decadal studies are mainly conducted in the European Alps (e.g., Kellerer-Pirklbauer and Kaufmann,[8] Kenner et al.,[9] Marcer et al.,[12] Avian et al.,[22] Dusik et al.,[23] Fleischer et al.,[24] Hartl et al.,[25] Kaufmann and Landstädter,[26] Kellerer-Pirklbauer and Kaufmann,[27] Lugon and Stoffel,[28] Roer,[29] and Scapozza et al.[30]) and also in other mountain regions such as the northern Tienshan,[31] the Andes of Chile,[32] Front Range, the United States,[33] or Iceland.[34,35] Because, with a few exceptions, multi-decadal kinematic time series of rock glaciers with geodetic methods are hardly available,[25,36] most studies employ a retrospective analysis of aerial photographs to derive information on flow velocities and surface elevation changes (e.g., Fleischer et al.,[24] Kellerer-Pirklbauer and Kaufmann,[27] Roer,[29] Kääb et al.,[31] Kaufmann et al.,[37] and Monnier and Kinnard[38]). In addition to rock glaciers, this method has been successfully applied to analyze the multi-decadal development of glaciers (e.g., Capt et al.,[39] Mertes et al.,[40] Midgley and Tonkin,[41] Mölg and Bolch,[42] and Vargo et al.[43]). However, this approach limits the period of observation to the earliest aerial photographs, which are available throughout the Alps from about the early 1950s onward. To our knowledge, the possibility of analyzing rock glacier kinematics by monoplotting on historical terrestrial images taken before the first aerial photographs has been explored only by Scapozza et al.,[30] probably due to the rarity of such images. With this exception, studies that examine the development of rock glaciers before 1953 tend to focus on the evolution of rock glaciers over thousands of years.[44,45]

Multi-decadal studies on the European Alps reveal a significant increase in flow velocities starting in the 1990s, accompanied by negative volume balances indicating thawing of permafrost ice.[8,24,37] Both observations are explained by an increase in ground temperature, which is largely a function of mean annual air temperature (MAAT) as well as the onset, duration, and depth of snow cover.[9,46,47] Furthermore, rock glacier kinematics are controlled by factors such as underlying bedrock topography; rheology of the frozen debris; ice and debris supply; spatiotemporal variations in ice content; thickness of the permafrost layer; and advection, infiltration, or internal production of water.[6,9,20,48–50] Besides the acceleration in the 1990s, some rock glaciers show increased flow velocities between the 1950s and 1970s compared to the subsequent periods that are associated with the decennial variations in the MAAT.[18,24,26,28]

Because a warm phase in the European Alps, which is a possible explanation for these increased flow velocities, was measured between the 1940s and the 1950s,[51] we see the necessity to investigate rock glacier evolution before the early 1950s (the time of the first aerial photographs) to better understand their response to this warm phase. In addition, a retrospective extension of the time series will bring us closer to the end of the Little Ice Age (LIA), which represents a starting point for massive system changes in the European Alps. This could improve our knowledge of the historic evolution of these landforms and in turn contribute to a better understanding of the current and the future development of rock glaciers. Thus, in this publication we focus on the utilization of a historical stereophotogrammetric map from 1922 (FW1922), produced by Finsterwalder,[52] and flow velocity profiles recorded stereophotogrammetrically by Pillewizer[53] between 1938 and 1953 to analyze the geomorphic development of the composite Innere Ölgrube rock glacier (OegRG) Kaunertal, Austria. The OegRG represents a rock glacier showing increased flow velocities between the 1950s and the 1970s[24] and is therefore assumed to show a distinct reaction to the warm phase of the 1940s to the 1950s. The evaluation of FW1922 allows us to investigate the changes in surface elevation and frontal advance, whereas the historic flow velocity profiles represent point measurements of the flow velocity before 1953. Both analyses are correlated with data derived from aerial photographs and airborne laser scanning (ALS) for several time periods between 1953 and 2017[24] and an additional ALS data set from 2021. In this way, a time series of the geomorphological development of the OegRG can be analyzed, and the development of the two lobes can be compared over a period of almost a century (1922–2021).

2 | MATERIALS AND METHODS

To characterize the evolution of the OegRG from before the first aerial photographs were taken until today, this study analyzed historical data and compared them with the available results (flow velocity and surface elevation change) from several time steps between 1953 and 2017.[24] In addition, the time series was extended by an ALS data set recorded in 2021. The historical data comprised a stereophotogrammetrically recorded map from 1922[52] and two stereophotogrammetrically measured flow velocity profiles between 1938–1939 and 1938–1953, respectively.[53]

2.1 | Study area

The OegRG is located in a small east–west oriented side valley of the Kaunertal, Ötztal Alps, Austria (Figure 1). The study area is climatically characterized by the central-alpine dry region.[54] At the Weißsee meteorological station (2,470 m a.s.l.), a MAAT of −0.11°C and annual precipitation ranging from 731 to 1,118 mm were recorded between 2007 and 2019 (data source: TIWAG—Tyrolian Hydropower AG).

The composite OegRG consists of two tongue-shaped adjacent rock glaciers separated by a medial moraine. Whereas the northern lobe (Lobe1) is glacier-forefield-connected, the southern lobe (Lobe2) represents a polyconnected rock glacier with an upslope connection to both a talus and a glacier forefield. Lobe1 is mainly composed of grayish weathered polymetamorphic gneisses derived from the steep headwall, whereas the smaller Lobe2 consists mainly of brownish weathered polymetamorphic schists derived from steep walls forming the small cirque at the northwestern side of the Wannetspitze.[55] Detailed information on geometry and other characteristics is provided in Table 1.

OegRG has already been the subject of several studies, including Hausmann et al.,[56] who used various geophysical methods to investigate the internal structure and ice content of Lobe1. The results indicate four layers consisting of 4–6 m of surface debris (active layer), 20–30 m of ice-rich permafrost, 10–15 m of ice-free sediments, and the underlying bedrock. They estimated the volumetric ice content to be 43% in the terminal part and 61% in the middle part. In the early- to mid-2000s, flow velocities of OegRG were determined using differential global positioning systems on multi-annual, annual, and seasonal bases, resulting in maximum flow velocities of 2.5 m/year and increased flow velocities during the melt season.[50,55,56] In recent years, the flow velocities of the rock glaciers in the Kaunertal have been determined using image correlation between 1953–2017[24] and 2001–2015.[57] In addition, the hydrology of the rock glacier and its springs has been investigated. This revealed distinct seasonal and diurnal variations in the discharge, the temperature of which is

FIGURE 1 (a) Overview map displaying the location of the Ölgrube rock glacier (OegRG) and the meteorological station in the Ötztal Alps, Austria. (b) Map of the studied OegRG, its catchment areas, and glacier cover at different years between Little Ice Age (LIA) and 2017 (see Section 2.5.1). In addition, the stable areas used for the uncertainty analysis are shown. (c) Photo of the OegRG facing east (photo by Anton Brandl, 2021) [Colour figure can be viewed at wileyonlinelibrary.com]
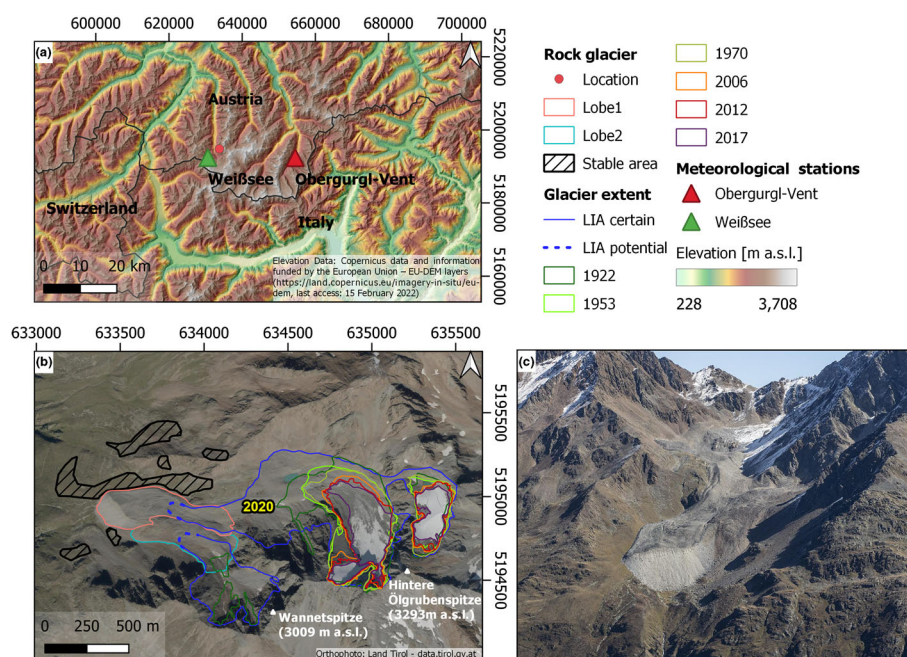
TABLE 1 Geometric and other characteristics of the OegRG in 2021

	Length (m)	Width (m)	Area (km²)	Elevationminimum	Elevationmaximum	Front height max (m)	Slope front(°)
Lobe1	~820	~180	0.13	2,454.4	2,758	~90	36.9
Lobe2	~610	~150	0.1	2,524	2,779.4	~60	37.4

Note: The elevation is the distance from GRS 1980 in meters.
Abbreviation: OegRG, Ölgrube rock glacier.

TABLE 2 Data used for mapping, surface elevation change, and flow velocity analysis

Date	Data type	Source	Point density(pt/m²)	Product	GSD[a] (m)	DEM cell size(m)	Analysis[b]
Mid-August 1922	Historic map	Finsterwalder[52]	–	Georeferenced map, DEM	–	5	1, 2
September 1 and September 8, 1953	Aerial images	BEV	6.4	DEM, Orthofoto	0.23	1/5[c]	1, 2, 3
September 29, 1970	Aerial images	Office of the Tyrolean Government-Department of Geoinformation	9.2	DEM, Orthofoto	0.19	1	1, 2, 3
September 13, 1982	Aerial images	BEV	–	Orthofoto	0.52	–	3
September 11, 1997	Aerial images	BEV	–	Orthofoto	0.56	–	3
September 5, 2006	ALS	Tyrolian Hydropower AG (TIWAG)	3.9	DEM	–	1	1, 2, 3
July 4, 2012	ALS	Chair of Physical Geographie University of Eichstätt-Ingolstadt	12.7	DEM	–	1	1, 2, 3
June 5, 2017	ALS	Chair of Physical Geographie University of Eichstätt-Ingolstadt	21.6	DEM	–	1	1, 2, 3
September 24, 2021	ALS	Chair of Physical Geographie University of Eichstätt-Ingolstadt	12.5	DEM	–	1	1, 2, 3

Note: Further information on processing of the historic map (FW1922) is provided in Section 2.3, whereas further information on processing of the aerial images and ALS data is found in Section 2.2 and Fleischer et al.[24]

Abbreviations: ALS, airborne laser scanning; DEM, digital elevation model; GSD, groud sampling distance.

[a]Ground sampling distance.

[b]1, mapping; 2, surface elevation change; 3, flow velocity.

[c]In the case of the DoD calculation 1922–1953, the DEM with a resolution of 5 m was used, whereas for the DoD calculation 1953–1970, the DEM with a resolution of 1 m was used.

permanently below 1.5°C.[55] Wagner et al.[13] describe the different flow paths within the rock glacier and underline its importance as a shallow groundwater aquifer.

2.2 | Processing of the historical aerial photographs and ALS data

The characteristics, processing, and uncertainty assessment of the historical aerial photographs and ALS data and their derivatives between 1953 and 2017 are described in detail by Fleischer et al.,[24] whereas a summary of all data used is provided in Table 2. The processing and analysis of the ALS data set from 2021, which was recoded on September 24, 2021, by the Chair of Physical Geography University of Eichstätt-Ingolstadt using the scanner model Riegl VuxSys-LR and achieving a mean point density of 12.5 pt/m^2 in the area of the rock glacier, was carried out analogously to these data. In summary, the historical aerial photographs were scanned at a resolution of 12 μm by the Office of the Tyrolean Government-Department of Geoinformation (1970) and 15 μm by the Austrian Federal Office of Surveying and Metrology (BEV) (1953, 1982, 1997). All aerial photos were provided in tiff format along with the camera calibration protocols, if available. Both the orthophotos and the digital elevation models (DEMs) were created with Agisoft Methashape (v.1.6.1) following the standard SfM-MVS workflow using the film camera option and the camera calibration protocols if available. After co-registration to the reference orthophoto (1953) and resampling of the orthophotos to a common resolution of 0.5 m, the orthophotos and, in the case of the ALS data hillshades with a resolution of 1 m, flow velocities were calculated in SAGA GIS using the Imcorr algorithm.[58] The algorithm uses a fast Fourier-transform-based version of a cross-correlation to correlate small sub-scenes from two images. In the case of moving landforms, such as rock glaciers, this produces vectors that represent the flow direction and flow distance between two images. In this study, search and reference window sizes of 256 × 128 and 128 × 64 with a fixed spacing of 5 m were used. Then, the resulting vectors were cleaned manually, and a level of detection (LoD) was determined based on the approach of Fey and Krainer.[59]

Both the SfM-MVS and ALS point clouds were thinned using the 3D block thinning tool in SAGA LIS (Laserdata GmbH, Innsbruck, Austria) to a uniform point spacing of 0.5 m. This step is necessary to achieve good results when fine-registering the point clouds to the reference data set (ALS 2017) using an iterative closest point algorithm.[60] Subsequently, the point clouds were gridded with a common resolution of 1 m, and DEMs of difference (DoDs) were calculated. These were then used to calculate surface elevation and volume changes in the OegRG.

2.3 | Stereophotogrammetric map from 1922

2.3.1 | Map creation

In the notes to the map of Gepatschferner, Finsterwalder[52] describes in detail how the stereophotogrammetric map of the Kaunertal was acquired and produced. For this purpose, 17 photographic images were taken with a phototheodolite on 12 days in mid-August 1922, and their locations were determined. The height of the images ranged from 1920 to 3,500 m a.s.l. with a baseline of 20–500 m.[52] The photographs were later analyzed stereophotogrammetrically, and a map of the entire upper Kaunertal was created at a scale of 1:10,000, which unfortunately has been published only at a scale of 1:20,000 with an isohypse equidistance of 20 m. The original photographs that were used to create the map and the original map could not be found, despite strong efforts and extensive research in private collections and archives. The classification of the scree signature was based on the photographs and can therefore be assumed to be accurate, so that the terminal part of the rock glacier can be distinguished from the front. Finsterwalder[52] describes that there was a long period of fine weather before and during the recording, which led to the firn fields below 3,300 m becoming snow free. The debris signature, the description of the period of good weather, and the detailed description of
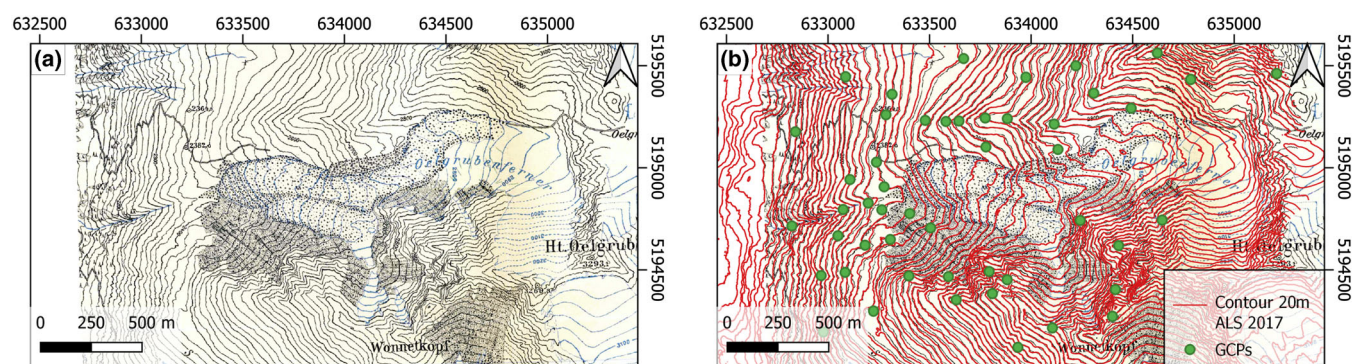
FIGURE 2 (a) Section of the FW1922[52] in the area of the Ölgrube rock glacier (OegRG). (b) FW1922 overlaid with corresponding contour lines derived from the ALS 2017 data set (red line) and ground control points (GCPs) placed at stable, distinct break points of these contour lines (green points). Three of the 52 GCPs are not visible in the map as they were placed outside the map area. [Colour figure can be viewed at wileyonlinelibrary.com]

the condition of the OegRG lead to the reasonable assumption that the study area was free of snow during the survey.

2.3.2 | Georeferencing and processing

Because the reference data set (ALS2017) is available in the coordinate system ETRS89/UTM zone 32N (EPSG 25832), the challenge was to georeference the historical map and to transfer it to this coordinate system. Several approaches were tried: (i) georeferencing by coordinate transformation of the fixed points marked on the map, (ii) georeferencing by analysis of local extreme values and inverse terrain models (local peaks and sinks), and (iii) calculation of the elevation difference between the reference data set and the elevations given in the map using fixed points and subsequently georeferencing at break points of the corresponding contour lines of the reference data set (Figure 2).

Because approaches (i) and (ii) produced unsatisfactory results, we used approach (iii) and describe it in more detail (Figure 3). The elevation difference was determined at 17 fixed points, and their mean value was used for the following adjustment in the elevations. Therefore, contour lines with an equidistance of 20 m were created from the reference data set (ALS2017), corresponding to the contour lines of FW1922. The map was then co-registered to the reference data set at 52 stable, distinct, and evenly distributed break points of these contour lines. Adjust was chosen as the transformation method and a root mean square error (RMSE) of ±1.39 m was achieved. This approach has the advantage of setting a larger number and better distribution of co-registration points around the area of interest compared to approaches (i) and (ii). After co-registration of the FW1922, the contour lines were manually vectorized and converted to a 5×5 m DEM using the Topo to Raster tool implemented in Esri ArcMap (v.10.6.1). This tool is based on the ANUDEM program developed by Hutchinson et al.[61] To minimize the uncertainty during

digitization of historical maps, both the interpretation of the signatures and the vectorization of the features were performed by one interpreter.[62] In a further step, the derived DEM was co-registered to the ALS2017 DEM using the python tool pybob,[63] which is based on the algorithm for iterative co-registration of DEMs proposed by Nuth and Kääb.[64]

2.3.3 | Uncertainty assessment

Regarding the uncertainty analysis for the volume changes, as for all DoDs presented in this paper, we followed the approach of Anderson,[65] who presented an error propagation method to derive the uncorrelated, correlated, and systematic errors and combine them into an overall uncertainty without applying a minimum LoD. Therefore, stable areas in the vicinity of the rock glacier were mapped and used to determine the uncertainties (see Figure 1 and Section 2.5.3).

According to Anderson,[65] the following formulas were used to determine the volumetric uncertainty.

In the case of uncorrelated random error:

$$\sigma_{v,re} = \sqrt{n}L^2\sigma_{RMSE} \qquad (1)$$

where n is the number of cells being aggregated, L is the cell size (m²) of the investigated area, and σ_{RMSE} represents the RMSE in stable areas.

In the case of spatially correlated random error:

$$\sigma_{v,sc} = 0.79a_i\sqrt{n}L\sigma_{sc} \qquad (2)$$

where a_i is the circular area over which errors are correlated (this represents the range of a spheric semivariogram model with no nugget) and σ_{sc} is the spatially correlated DoD uncertainty (m).

In the case of systematic error:

$$\sigma_{v,sys} = nL^2\sigma_{sys} \qquad (3)$$
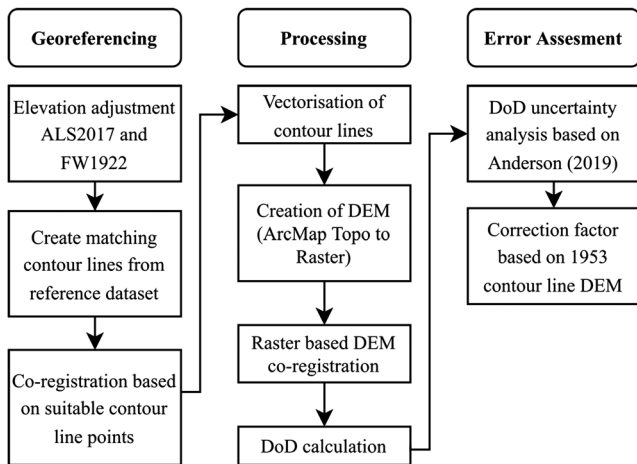
where σ_{sys} is the mean value in stable areas.

To estimate the total volumetric uncertainty (σ_v), Formulas 1–3 are combined:

$$\sigma_v = \sqrt{\sigma_{v,re}^2\sigma_{v,sc}^2\sigma_{v,sys}^2} \qquad (4)$$

For map representations of the surface elevation changes (Figure 5), a $_{min}$LoD was calculated using the same stable areas as for the volumetric uncertainty calculation. $_{min}$LoD was calculated following probabilistic thresholding, applying a user-defined confidence interval of 95% ($t_{crit} = 1.96$)[66]:

$$_{min}LoD = t_{crit}\delta_{DoD} \qquad (5)$$

where δ_{DoD} is the standard diviation of error measured in stable areas.

Georeferencing

| Elevation adjustment ALS2017 and FW1922 |
| ↓ |
| Create matching contour lines from reference dataset |
| ↓ |
| Co-registration based on suitable contour line points |

Processing

| Vectorisation of contour lines |
| ↓ |
| Creation of DEM (ArcMap Topo to Raster) |
| ↓ |
| Raster based DEM co-registration |
| ↓ |
| DoD calculation |

Error Assesment

| DoD uncertainty analysis based on Anderson (2019) |
| ↓ |
| Correction factor based on 1953 contour line DEM |

FIGURE 3 Workflow diagram of FW1922 georeferencing, processing, and error analysis. The individual processing steps are explained in more detail in the text

To estimate the transformation uncertainty on the complex terrain of the rock glacier caused by the interpolation of the contour lines, which is not found to this extent on the stable reference surfaces, further analyses were immediately required. Based on the DEM of 1953, a 5×5 m grid DEM derived from the point cloud was compared with a model created from 20 m contour lines of the same data set. The difference between the parameters calculated on stable areas and the respective area of the rock glacier from this DoD was applied as correction factors when calculating the uncertainties and the LoD of the DoD 1922–1953 in the respective areas. The valid determination of such a correction factor presupposes that the topography of the rock glacier does not change, which it does to a certain degree. Therefore, the 1953 data set was preferred to the reference data set (ALS2017) for the analysis, as it is closest to 1922 and thus has the most similar topography.

2.4 | Historical flow velocity profiles

In 1938, Pillewizer established two stereophotogrammetric motion profiles on stone lines, remeasuring Profile1 in 1939 and Profile2 in 1953. Unfortunately, the measuring point of the first profile could not be found in 1953, making remeasurement impossible. To enable a comparison of the flow velocity profiles with the measurements carried out after 1953 using image correlation analysis,[24] the map was georeferenced to the FW1922 using 30 reference points in and around the rock glacier, achieving an RMSE of ±0.89 m. Using points within the rock glacier is a valid approach, as Pillewizer[53] uses Finsterwalder's[52] map to visualize the flow velocity profiles. Subsequently, the profile lines were digitized. In a further step, the flow velocity diagrams published by Pillewizer[53] were measured using the drawing program Inkscape to calculate the exact point localities and measurement results at these points.

2.5 | Mapping

2.5.1 | Glacier extent

The glacier evolution was primarily reconstructed to assess the approximate glacier extent at the end of the LIA and to be able to depict the glacier development in the catchments of the two lobes during the study period (Figure 1). Abermann et al.[67] have highlighted the potential of high-resolution DEMs to mapping glacier outlines, which has been adopted by several studies on individual glaciers (e.g., Klug et al.[68]) or entire mountain ranges (e.g., Fischer et al.[69]). Following this published approach, we utilize DEMs (and their derivatives) derived from ALS data (2017 and 2006: Office of the Tyrolean Government, Department of Geoinformation/Tyrol, Austria; 2012: PROSA [PROglacial Systems of the Alps] project) and photogrammetric techniques (1953 and 1970: aerial photographs; see Section 2.2). ALS-DEMs were further used to digitize the LIA extent by morphological mapping of moraines, which were additionally confirmed by

orthophotos and field observations. However, only the position of the maximum glacier extent at the glacier front can be estimated, as clear features have been erased by the moving rock glacier. As historical maps provide the opportunity to conduct area-wide glacier reconstructions (e.g., Freudiger et al.,[62] Rastner et al.,[70] Salerno et al.[71]), the mapping of the 1922 glacier margin was carried out based on the FW1922 map (see Section 2.3.2).

2.5.2 | Stable areas

Stable areas were mapped to (i) fine-register all available point clouds (see Section 2.2) and (ii) to determine the uncertainties of the volumetric changes and the LoD (see Section 2.3.3). To ensure that the uncertainty analysis is not performed exclusively on the areas used for fine-registration, stable areas of (i) and (ii) differ, with those used for (i) shown in Figure 1.

For the selection of the stable areas, we excluded all areas with slopes greater than 40° due to the strong correlations between slope and elevation uncertainties in both ALS[72] and SfM-MVS DEMs.[73] In addition, the selection is constrained by the requirement that the areas should be as large and coherent as possible and cover many slope aspects to ensure a good fit of the point clouds[74] and an accurate determination of the correlated random error with a large correlation range.[65] Therefore, co-registered orthophotos and initial DoDs without fine-registration were used to map stable areas. The requirements for stable areas and the terrain in the vicinity of OegRG led to alpine grassland being mapped as stable in addition to bedrock and scree areas. The fact that the data were taken at approximately the same time of year and that the DoDs show no difference between stable alpine grassland and bedrock areas made this approach valid.

2.5.3 | Rock glacier front

The fronts of the two rock glacier lobes were mapped according to the IPA Action Group Rock Glacier Inventories and Kinematics—Towards Standard Guidelines for Inventorying Rock Glaciers: practical concepts (version 2.0).[75] A distinction was made between the restricted outline, which excludes the frontal talus of the rock glacier and represents the front line of the rock glacier, and the extended outline, which represents the base of the frontal talus or, with changing frontal slope angles, the shear zone. In the case of 1922, mapping of the rock glacier front was based on the FW1922, where a change in the scree signature allows the distinction between the main body of the rock glacier (restricted outline) and the steep front (extended outline). For Front2, the change in the signature is not clear, which is why the restricted outline of the front cannot be mapped unambiguously. For the following six time periods between 1953 and 2021, the front was mapped based on the respective hillshade and slope grid (e.g., Abermann et al.[67] and Janke[76]). In addition, the volume change of the front was calculated to better characterize the frontal advance.

This was done considering the blocky rock glacier forefield to account for volume change that can occur due to mass movements like rockfall or debris flows on the steep rock glacier front.
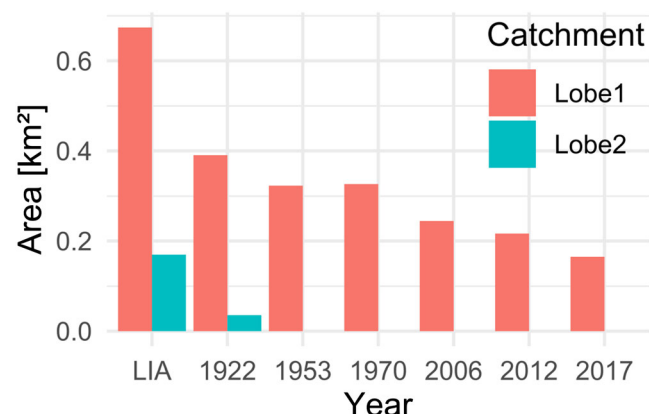
FIGURE 4 Glacier area (km²) of the two catchment areas of Lobe1 and Lobe2 of the Ölgrube rock glacier (OegRG) [Colour figure can be viewed at wileyonlinelibrary.com]

2.6 | Climate data

The primary aim of this study is a long-term description of rock glacier development. Nevertheless, the annual temperature and temperature anomaly of the meteorological station Obergurgl-Vent (1938 m a.s.l.) between 1920 and 2021 were analyzed to identify correlations between temperature development and rock glacier evolution. These data were provided by the Historical Instrumental Climatological Surface Time Series of the Greater Alpine Region (HISTALP). The station is located 20.8 km from the survey area in the Gruglertal, Austria, and is elevated ~450 m lower than the front of the rock glacier (Figure 1).

3 | RESULTS

3.1 | Glacier area change

The glaciated area in both catchments (Lobe1 and Lobe2) of the OegRG is shown for different years between the LIA and 2017 in Figures 1 and 4. During the LIA, the two rock glacier lobes were at
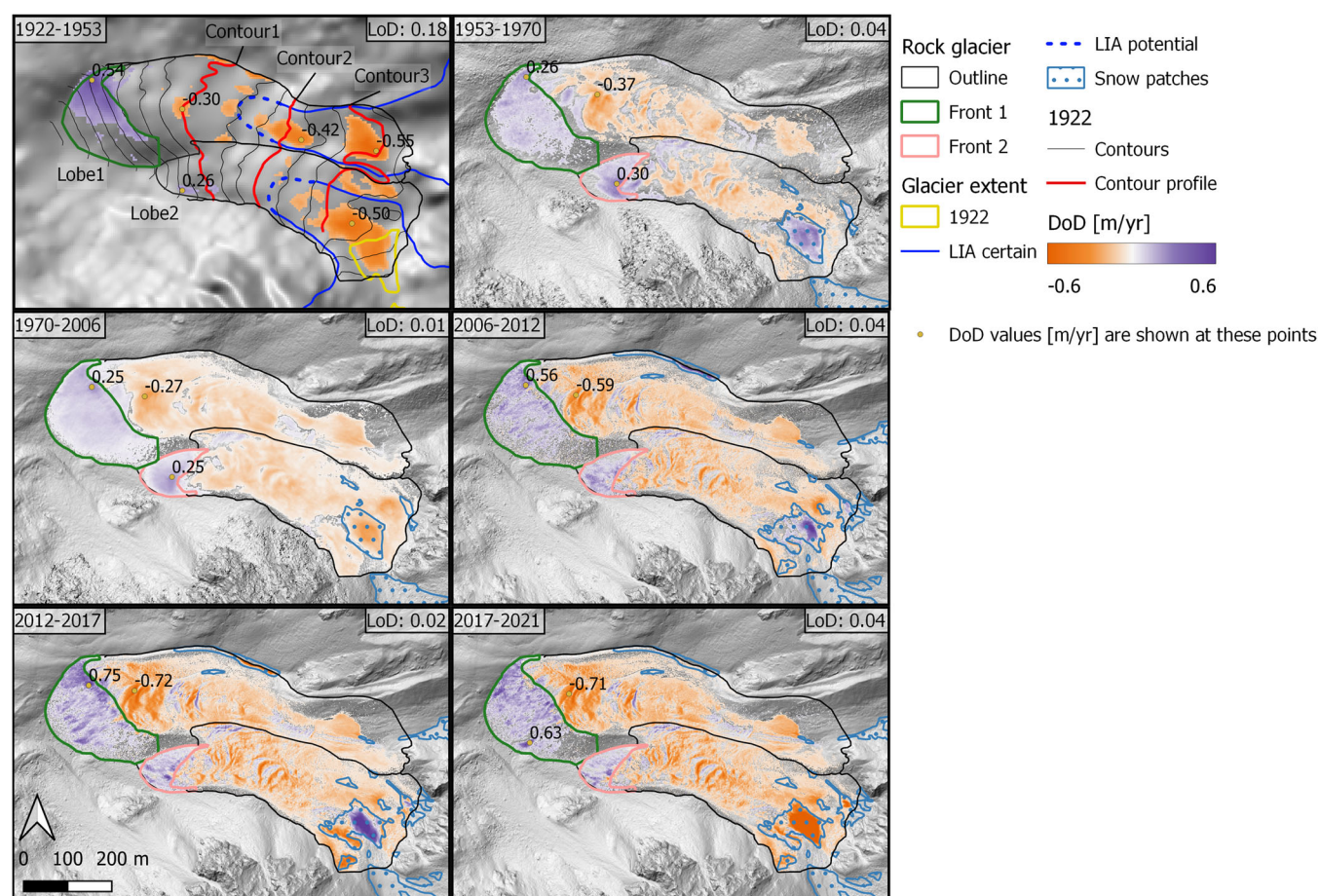
FIGURE 5 Maps of the Ölgrube rock glacier (OegRG) showing the mean annual surface elevation change for six time steps between 1922 and 2021. Front1 (dark green) and Front2 (pink) show the areas used for volume calculation of the fronts, which include the blocky rock glacier forefield and therefore differ from the fronts in Figure 9, which show only the steep front. The rock glacier outline (black) shows the area of Lobe1 and Lobe2, which was used for the respective volume calculation of the time step in addition to the respective frontal areas. The point values of the surface elevation change in the individual time slices (m/year) reflect the maximum and minimum values. DoD values below the respective LoDs are not shown in the figure. [Colour figure can be viewed at wileyonlinelibrary.com]

least partially overprinted by glaciers. Due to the intense melting of the glacier ice, no direct contact between the rock glacier and the glaciated area was observed in 1922. By 1953, the glacier in the catchment of Lobe2 already melted completely. In the case of the glacier in the Lobe1 catchment, the average annual area loss between LIA and 1922 was significantly higher, with −4,234 m^2/year than with −2,168 and −2,283 m^2/year in the subsequent periods 1922–1953 and 1970–2006, respectively. The highest average area loss of −10,344 m^2/year was recorded between 2012 and 2017, whereas a slight area gain of 210 m^2/year was observed between 1953 and 1970.

3.2 | Surface elevation change

Both positive- and negative surface elevation changes were observed on the rock glacier in all time steps. For the DoD between 1922 and 1953, a corrected LoD of ±5.74 or ±0.18 m/year was determined. For a better representation of the significant surface elevation changes in Figure 5, values below this LoD are not shown. Nevertheless, an area with positive values can be observed in Front1, with a maximum of 16.84 m (0.54 m/year). Especially in the upper part of both rock glacier lobes, the DoD revealed large areas with negative values up to −17.01 m (−0.55 m/year). However, the resolution of the 1922 DEM was not sufficient to represent the complex topography of the rock glacier, for example, smaller flow bulges. In the five time periods between 1953 and 2021, the DEMs obtained using SfM-MVS of historic aerial images and ALS data allowed for a more differentiated representation of the surface elevation changes due to the better resolution and accuracy.[24] The LoDs in these time periods were between ±0.01 and ±0.04 m/year and therefore significantly better than those in the time period 1922–1953, which included the DEM calculated from the contour lines of the FW1922. In addition to the positive values at the rock glacier fronts and the negative values over extensive areas, the time slices since 1953 therefore also showed positive values, for example, at the flow bulges of the rock glacier. In parts, the areas with large negative values in the DoD 1922–1953 were also detected in the subsequent periods, although with significantly lower values. Maximum values of the negative surface elevation change were identified in all time periods between 1953 and 2021 in the terminal area of the rock glacier Lobe1.

In addition to the surface elevation change maps (Figure 5), which illustrate the spatial distribution of the changes well, profiles of the DEMs along the contour lines of the FW1922 were established; these show the temporal development of surface elevation (Figure 6). This approach eliminated some of the uncertainties that exist due to the interpolation between the contour lines in the case of the 1922 DEM and therefore corroborated the observations that were made in the DoD 1922–1953.

The elevation profiles are difficult to interpret due to the nonlinearity of the contour lines and the various processes that can lead to positive and negative surface elevation changes. Nevertheless, for the areas of the contour line passing through the upper part of the OegRG, areas that show a strong subsidence of up to −15.26 m between 1922 and 1953 were identified. In addition, areas of moderate but more extensive subsidence were recognized. In the case of Contour1, increasing values compared to 1922 indicated an advance in Front2.

3.3 | Volume balance

When deriving the positive- and negative surface elevation changes and the resulting volume balances, the snow-covered areas were masked out for all epochs to ensure comparability (Figure 5). Therefore, and because melting and refreezing of ice in pore spaces are not reflected by the surface elevation change, one cannot speak of a mass balance in the strictest sense. Nevertheless, the temporal comparison of the rock glacier volume changes allowed for interpretations.
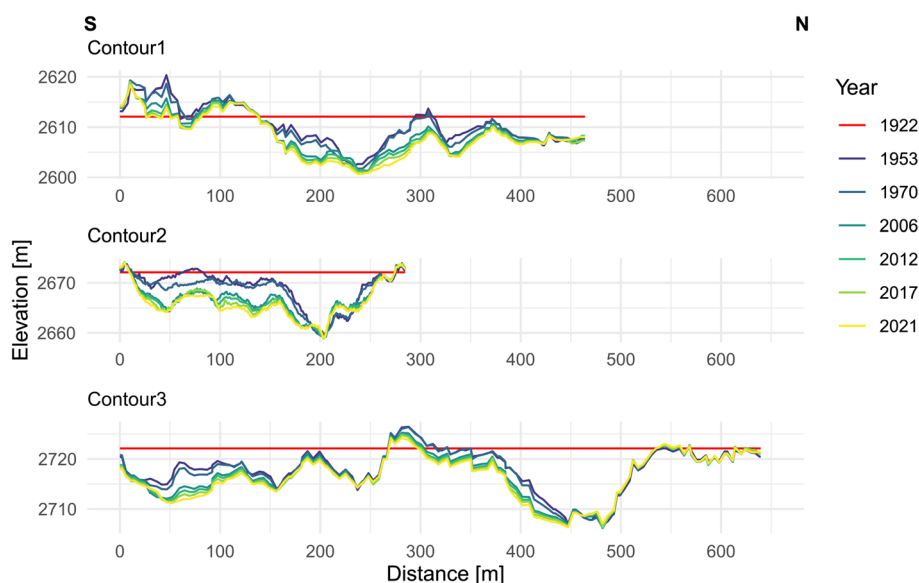
FIGURE 6 Elevation profiles at three contour lines of FW1922 for 7 years between 1922 and 2021 surrounding the rock glacier. The elevation is given in meters above GRS80, and in relation to distance it is superelevated five times. The position of the contour lines is shown as a red line in Figure 5 [Colour figure can be viewed at wileyonlinelibrary.com]

The uncertainties of the annual net volume changes range from ±12.27 to ±275.88 m^3/year for the time slices between 1953 and 2021 and were considerably higher in the period 1922–1953, where they ranged from ±1,154.26 to ±2,570.15 m^3/year. Because these are given as mean annual uncertainties, they appear small in time slices in which the respective DEMs are temporally far apart.

In all time slices of the study period between 1922 and 2021, only negative volume balances occurred in the two lobes of the OegRG (Figure 7). Both positive- and negative volume changes were at a higher level in the time slice 1922–1953 than in the subsequent time slice 1953–1970. This was particularly pronounced in Lobe1 and here especially in the positive volume changes. From the time period 1953–1970 onward, the negative volume balances increased continuously until the most recent time period between 2017 and 2021, albeit with different magnitude when comparing the two lobes.

For a direct comparison of the two lobes, it is useful to consider the mean surface elevation change instead of the volume balance, as in this way the different surface areas are considered (Figure 5). On average, subsidence rates of only a few centimeters per year were measured, ranging between 0.01 and 0.07 m/year. Lobe1 showed relatively constant values in the three time periods between 1922 and 2006 and then a sharp increase in negative values and again relatively constant values in the three time periods until 2021, whereas Lobe2, after a decline in between 1922–1953 and 1953–1970, showed an increase in negative values from time step to time step until 2021.

3.4 | Change in rock glacier fronts

Between 1922 and 1953, the front position of Front1 changed drastically in the northern, topographically confined part. During this period, the upper front in that area was displaced by up to 34 m and the lower front by up to 17 m. In the following epochs, the greatest changes were also observed in this area of Front1, although to a much
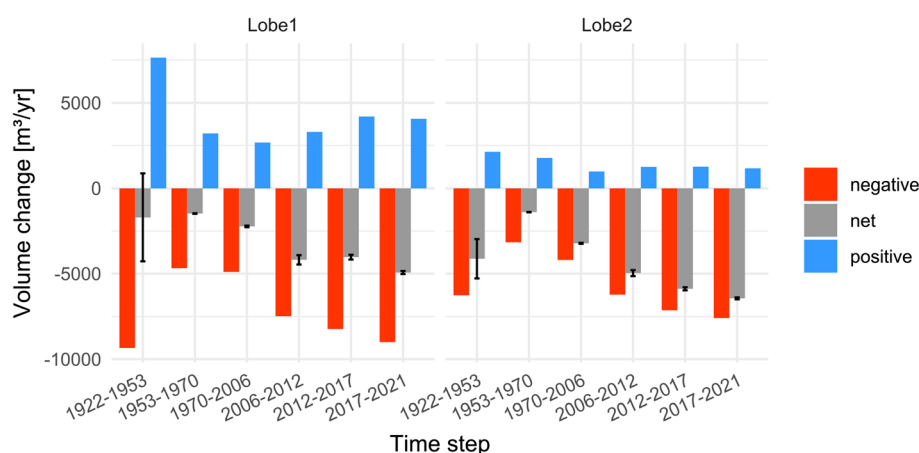
FIGURE 7 Mean annual volume change in both lobes of the Ölgrube rock glacier (OegRG) for six time steps between 1922 and 2021. The uncertainties (black indicators) were determined according to Anderson[65] [Colour figure can be viewed at wileyonlinelibrary.com]
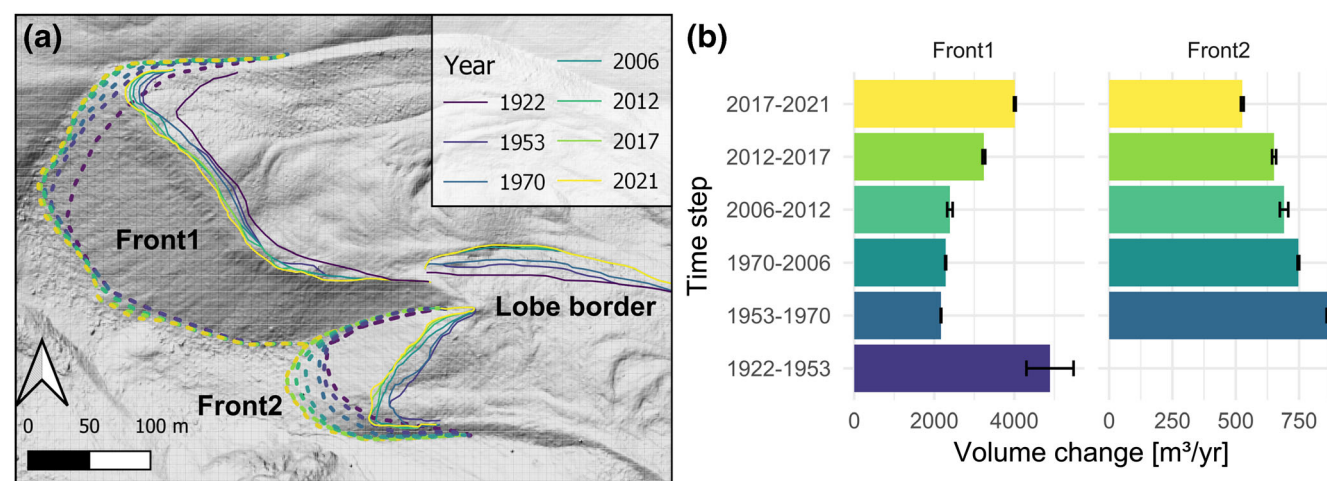
FIGURE 8 (a) Position of the upper (solid line) and the lower front (dashed line) of the two rock glacier lobes and the border between those lobes in seven epochs between 1922 and 2021. (b) Mean annual volume change in Front1 and Front2. The areas used for the calculation differ from the positions of the front in this figure because the blocky rock glacier forefield was included to consider volume changes due to mass movements at the front, such as rockfall (shown in Figure 3) [Colour figure can be viewed at wileyonlinelibrary.com]

lesser extent than between 1922 and 1953. Apart from this area, the lower part of Front1 hardly changed its position, whereas the upper part advanced by an average of ~15 m during the entire study period between 1922 and 2021. The greatest volume change in Front1 of 4,890.78 ± 588.77 m³/year was measured in the period 1922–1953. In the following period, the volume change decreased sharply, to increase slowly until the period 2006–2012 and more rapidly from that time onward (Figure 8b).

Considering the change in front position, Front2 showed a relatively homogeneous advance of the lower and upper front lines in the areas not constrained by Front1. In contrast to Front1, there was a clear advance of the lower front line over time, which resulted in a front advance of ~40 m between 1922 and 2021 in Front2. The volume changes in Front2 exhibited a contradictory pattern to Front1. Although no volume change was calculated for the area of the front in the first time step due to the fact that no unambiguous mapping of the upper position of the front was possible in 1922, the positive annual volume changes in the entire rock glacier indicated that it was slightly higher than that in the time period 1953–1970 (see Figure 7). From this point onward, a decrease from 862.45 ± 3.74 m³/year in 1953–1970 to 525.94 ± 5.38 m³/year between 2017 and 2021 was recorded.

The rock glacier changed its extent in the fronts as well as at the boundary of Lobe1 and Lobe2. Multi-temporal mapping of this boundary showed that Lobe2 moved north to northwest overriding Lobe1 by ~25 m between 1922 and 2021, causing the boundary between the two lobes to shift (Figure 8a).

3.5 | Flow velocity

The flow velocity showed a similar general spatial pattern on both lobes of the OegRG, with the highest values at the terminal part and continuously lower values in the upper parts of the rock glacier (Figure 9).

Concerning the temporal development in flow velocities, both lobes followed a similar general trend, although slight differences in temporal and spatial variation in flow velocities were observed. The general trend for OegRG was described in Fleischer et al.[24] and was expressed in increased flow velocities in the time period 1953–1970 compared to the two subsequent time periods between 1970 and 1997, followed by an acceleration with maximum flow velocities recorded in the time step 2012–2017. The largest accelerations as well as decelerations in flow velocity between the time steps were observed in most cases at both rock glacier fronts.

Analysis of the additional ALS data set from 2021 revealed a decrease in flow velocities between 2012–2017 and 2017–2021 of the terminal parts, which was particularly pronounced in the terminal
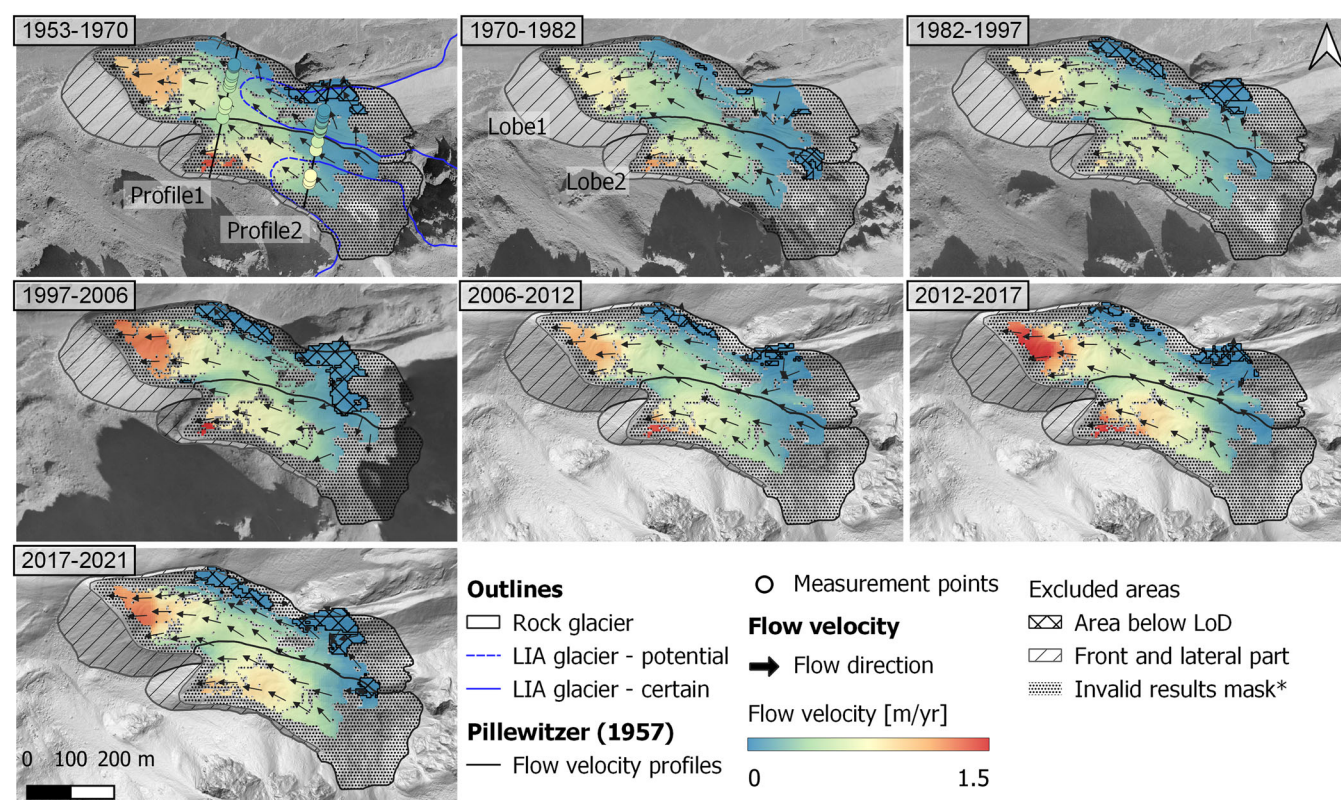
FIGURE 9 Flow velocity maps of the Ölgrube rock glacier (OegRG) for seven time steps between 1953 and 2021. The map of the 1953–1970 time step shows the profile flow velocity measurements made by Pillewizer[53] between 1938–1939 (Profile1) and 1938–1953 (Profile2). *Areas where no valid flow velocity measurement was possible due to snow, shadows, or erroneous image correlations in one or more time slices [Colour figure can be viewed at wileyonlinelibrary.com]

part of Lobe2. Here, the flow velocity decreased by up to −0.5 m/year. On the contrary, slight increases in a few centimeters per year were observed in the upper parts of Lobe2.

The two lobes differed slightly in the areal proportion and magnitude of the velocity increase and decrease between the time steps. This resulted in a larger area of Lobe2 having a higher velocity over time, especially from the 1997–2006 period onward. This was also reflected in a significant increase in the median flow velocity of Lobe2 from 0.36 m/year in 1982–1997 to 0.55 m/year in 2017–2021, whereas the median of Lobe1 remained almost constant over the same time periods (0.24 m/year in 1982–1997 and 0.29 m/year in 2017–2021) (Figure 10).

In addition to the area-wide flow velocities, which could be determined only for the periods between 1953 and 2021 using image correlation, historical recordings of flow velocities before 1953, carried out photogrammetrically by Pillewizer[53] on two profiles, were analyzed (Figures 9 and 11). Profile 1, covering the time between 1938 and 1939, was located on the central part of Lobe1 and showed similar or, in parts, even slightly higher values to recent time steps. Profile2 covered the period between 1938 and 1953 and was measured on the upper part of Lobe1 and Lobe2. In the area of Profile2 located on Lobe2, flow velocities of 0.75 m/year were measured during this period, which slightly decreased toward the boundary to Lobe1, amounting to 0.55 m/year. On average, these flow velocities were 0.26 m/year higher than the corresponding maximum flow velocities in this area between 1953 and 2021.

Although not as pronounced as on Lobe2, some measuring points on Lobe1 also showed a slightly increased flow velocity between 1938 and 1953 compared to the flow velocities between 1953 and 2021. The flow velocity on Lobe1 decreased significantly toward the margin and in this area no longer exceeded the values measured in the time periods between 1953 and 2021 (Figure 11).

Even though this statement can be made only for a few measuring points, the reanalysis and comparison of the historical flow velocity measurements of Pillewizer[53] indicated that some areas, in particular of Lobe2, had a higher flow velocity during the period from 1938 to 1953 than in the subsequent epochs up to 2021.

4 | DISCUSSION

4.1 | Uncertainties of historical data

4.1.1 | Stereophotogrammetric map from 1922

The uncertainties that resulted from the analysis of the FW1922 comprise various sources of error, which in some circumstances are propagating and can hardly be quantified. In addition to other sources of error, such as distortions of the original map caused by scanning, age, and humidity, these are primarily uncertainties in the (i) positioning of the photographs and their stereophotogrammetric processing used for map creation, (ii) georeferencing of the map, and (iii) creation of a DEM from contour lines and analysis of surface elevation changes including this DEM. In the case of point (i), there is no personal control over data acquisition and processing when utilizing historical data. Although Finsterwalder[52] stated an average positional accuracy of the photo locations in the xy-direction (±0.5 m) and in height (±0.3 m), this was not differentiated for the various images, and it was not possible to quantify how these errors affect the stereophotogrammetric processing. However, because Finsterwalder[52] described the OegRG in detail in his publication of the map, we assumed that the image
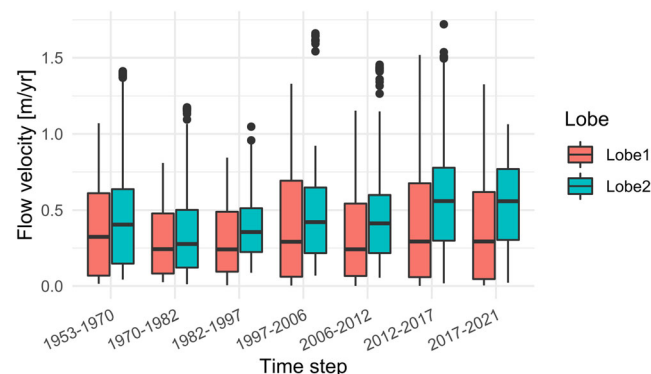
FIGURE 10 Boxplot of flow velocity of Ölgrube rock glacier (OegRG) for seven time steps between 1953 and 2021, subdivided by lobe. The bold black lines indicate the median values [Colour figure can be viewed at wileyonlinelibrary.com]
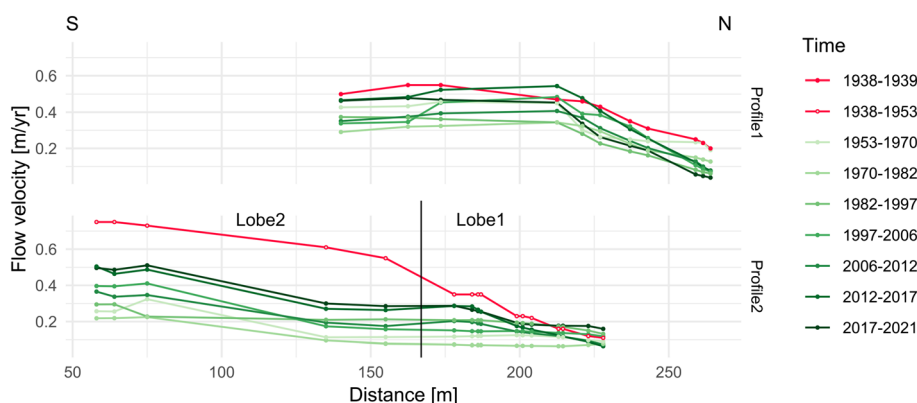
FIGURE 11 Diagram of the flow velocity profiles measured by Pillewizer[53] and flow velocity determined by image correlation at these points. The locations of flow velocity profile lines and measured points are shown in Figure 9 [Colour figure can be viewed at wileyonlinelibrary.com]

acquisitions and their stereophotogrammetric processing in this area were also carried out with a high degree of precision. For this reason, we assumed that the scree signature was created with great accuracy in the area of investigation. Source of error (ii) could be minimized by the applied georeferencing method and amounts to an RMSE of 1.39 m for the 52 georeferencing points used (see Section 2.3.2). In the case of point (iii), the error resulting from the interpolation between the contour lines was specified (see Section 2.3.3). However, as the correction factor was determined using the 1953 DEM, it should be considered as an estimate rather than a measurement of this error. Considering all these points, we consider the results obtained to be plausible and valid, although it should also be noted that not all sources of error regarding the FW1922 could be excluded or quantified.

4.1.2 | Historical flow velocity profiles

The previously described uncertainties, which must be considered when using historical data, are also found in the evaluated velocity profiles of Pillewizer.[53] In this case, the publication does not provide an estimate of the error caused by the positioning uncertainty of the photographs and their stereophotogrammetric processing. Because this could not be determined retrospectively, assumptions had to be made about the accuracy of the measurements. In the case of Profile1, we suspected that the short temporal baseline of only 1 year was associated with a high relative annual error due to measurement inaccuracies compared to the measured velocities. Therefore, the validity of the comparison with the following flow velocities is reduced. In contrast, the long temporal baseline of 15 years in the case of Profile2 suggests relatively small relative annual errors and thus, in our view, allows a comparison with subsequent flow velocities.

## 4.2 | Surface elevation and volume changes

The surface elevation change in rock glaciers reflects the sum of the strain pattern (compression and extension), downslope movement, compaction, debris input, and aggradation and melting of excess ice. Positive values occurred at both fronts and indicated a frontal advance. In addition, positive values appeared at the fronts of flow bulges and in the overthrust zone of Lobe2 and Lobe1, indicating compressive flow in these areas. The high negative values that occurred on the terminal part of Lobe1 can be explained, among other factors, by extensive flow, as Hausmann et al.[56] were able to detect a step in the bedrock topography beneath the rock glacier in this area using geophysical methods. As the investigated rock glacier lobes do not end above very steep terrain, there is no sediment output from the rock glacier system apart from the fine fraction. The consistently negative volume balances during the investigation period thus indicate, in addition to the compaction of debris, particularly the melting of excess ice.

The results of the surface elevation change between 1922 and 1953 indicated a considerable advance of Front1 during this period and an extensive subsidence in the upper parts of both rock glacier lobes. The effect of this is that the net volume change in the period 1922–1953 was at least as negative as in the period 1970–2006 on Lobe2, considering uncertainty. This statement cannot be made for Lobe1 due to the high degree of uncertainty and the large positive volume change that reduced the net volume balance. The areas showing large-scale subsidence were located within the maximum glacier extent of the LIA. Together with the results of the contour profile analyses, this indicated that these areas are probably debris-covered dead ice bodies, which likely developed from the debris-covered parts of the LIA glacier (for further discussion see Anderson et al.[77] and Deline[78]). After the retreat of the glacier, these successively melted, particularly strongly during the short warm phase between 1946 and 1951. Some of these dead ice bodies have already completely melted and formed depressions in the period 1953–1970, whereas others still show subsidence today, albeit weakened compared to 1922–1953. These observations in the DoD are confirmed by *in situ* observations by Berger et al.,[55] who found deep meltwater lakes in the upper part of Lobe2, indicating a massive ice body, and further discuss the glacial origin of OegRG. The interaction between rock glaciers and LIA glaciers, the resulting presence of massive glacial ice superimposed on the permafrost, and the preservation of this ice since at least the end of the LIA have also been demonstrated by Lugon et al.[79] for rock glaciers in the Posets massif, Central Pyrenees, Spain, and by Ribolini et al.[80] for the Schiantala Valley, Maritime Alps, Italy. An increased melting of the permafrost ice due to higher temperatures between 1946 and 1951 could also play a role in the strong negative volume balance between 1922 and 1953 (Figure 13). This could be particularly relevant for Lobe2, which, in contrast to Lobe1, showed a clear increase in negative mean surface change over the period 1970–2006 and therefore a faster or stronger response to the temperature increase from the mid-1980s onward. This is also shown by regression analysis, which shows a significant correlation between surface elevation change and MAAT for both lobes (Figure 12). Both the slope and the intercept are significantly steeper and lower in the case of Lobe2 with −0.023 and 0.0012 than in the case of Lobe1 with −0.013 and 0.0072.

For the period from 1953 onward, when comparable studies exist in the European Alps, the value ranges of mean surface elevation change are in line with those investigations. For example, Kellerer-Pirklbauer and Kaufmann[8] determined values between −0. 016 and −0.058 m/year for Hinteres Langtalkar rock glacier, Austria, between 1954 and 2012; Kaufmann et al.[37] derived values between 0.0008 and −0.013 m/year for Tschadinhorn rock glacier, Austria; and Fleischer et al.[24] determined values ranging between −0.047 ± 0.001 m/year and 0.005 ± 0.003 m/year for several rock glaciers in Kaunertal, Austria, between 1953 and 2017. The trend of increasing negative values observed on the two lobes of the OegRG in the time slices after 1953 was also observed by Fleischer et al.[24] for several rock glaciers in the Kaunertal, Austria, and by Kellerer-Pirklbauer and Kaufmann[8] for Hinteres Langtalkar rock glacier, Austria. However, the
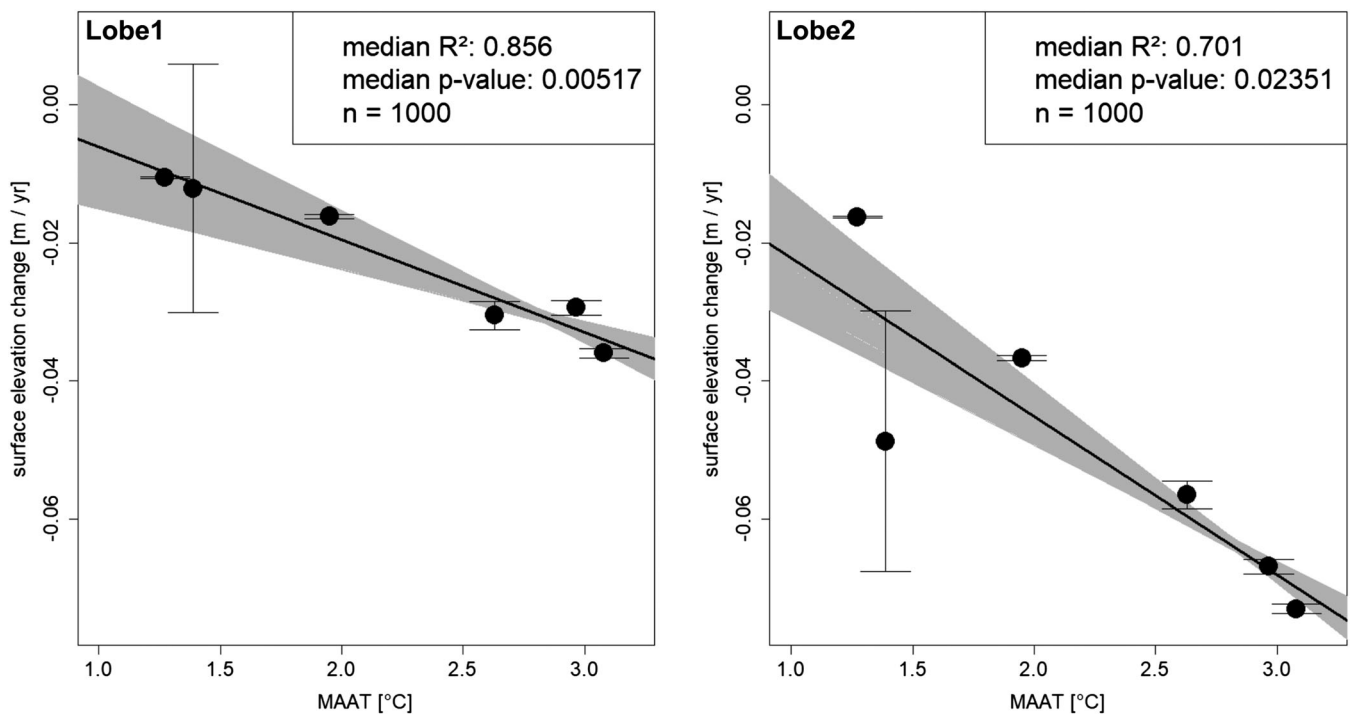
FIGURE 12 Bootstrapped regression analysis of mean surface elevation changes and mean annual air temperature (MAAT) for Lobe1 and Lobe2 of Ölgrube rock glacier (OegRG), which consider the uncertainties of the surface elevation measurement. Random values were determined within the uncertainty ranges of the individual values, and a regression was calculated. This process was then repeated 1,000 times; the black line represents the median of these regressions
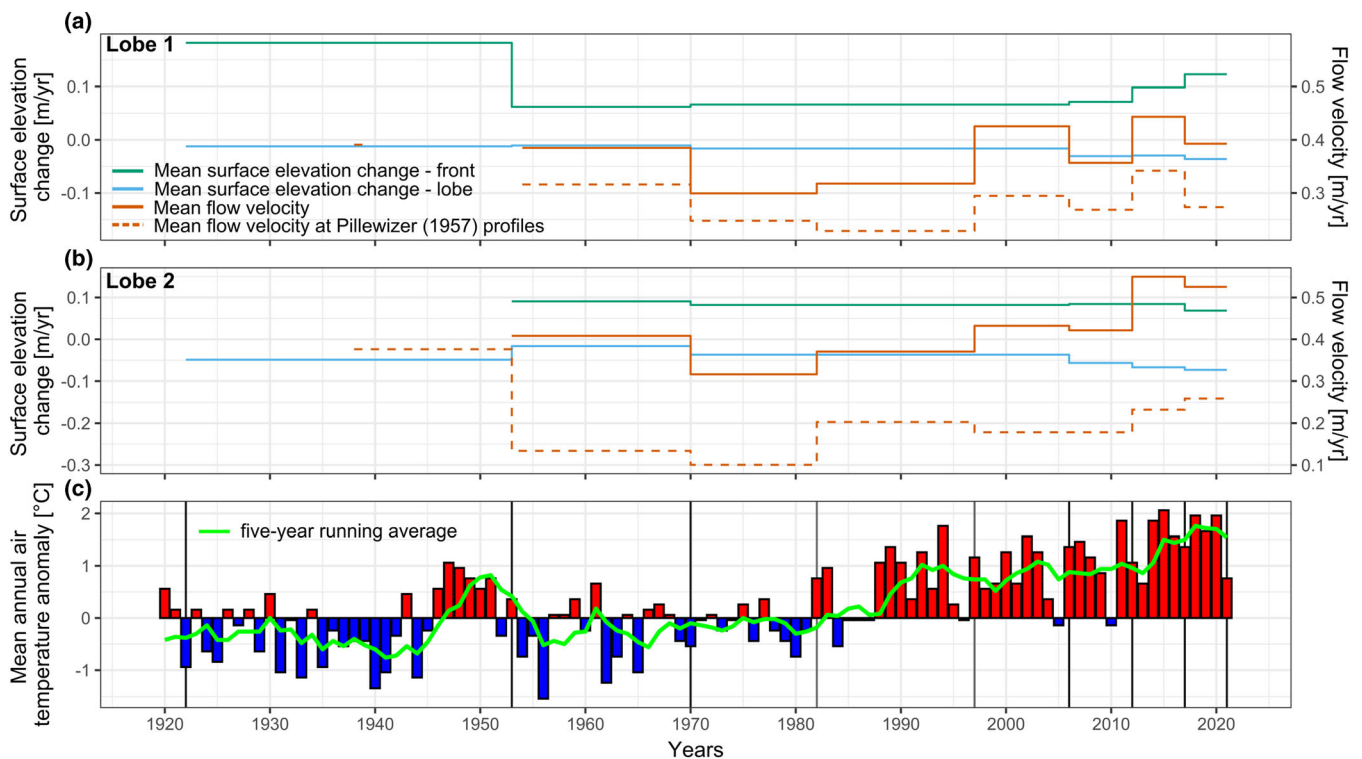
FIGURE 13 Mean surface elevation changes and mean flow velocities of the Ölgrube rock glacier (OegRG) differentiated by (a) Lobe1 and (b) Lobe2 in the different time periods. (c) Mean annual air temperature anomaly at the meteorological station Obergurgl-Vent (1938 m a.s.l.). The reference period for anomaly calculation is 1961–1990. Black and gray vertical lines indicate the time steps analyzed. Spatially better differentiated information on the analyzed parameters is shown in the previous figures [Colour figure can be viewed at wileyonlinelibrary.com]

Tschadinhorn rock glacier showed increasing negative values between 1954 and 2009 but a value close to zero between 2009 and 2015.[37] As stated earlier, the negative mean surface elevation changes in these rock glaciers indicate a melt out of excess ice. This can be explained by increasing temperatures since the mid-1980s (Figures 12 and 13), which, among other factors, led to a warming of permafrost and active layer thickening.[81] Although both lobes of OegRG showed negative values during the entire study period of 1922–2021 and followed a decreasing trend, there were also differences in the temporal development, especially between 1922 and 1953, but also in the following periods. Whereas Lobe1 showed a sharp increase in negative values only between 2006 and 2012, this can already be observed for Lobe2 in the period 1970–2006. Furthermore, the negative value of Lobe1 remained relatively constant in the following epochs, whereas it became increasingly negative in the case of Lobe2. because the external forces of the two lobes were almost identical, deviation in the temporal development might be attributed to differences in internal structure (ice content) or to the sensitivity of the contained ice to external effects.[3]

4.3 | Mechanisms of frontal advance

The front advance of a rock glacier is a function of the compaction of debris, the vertical variation in the horizontal flow velocity, and the volume change due to ice melting.[82] In special cases where rock glaciers terminate over steep terrain,[83] erosion and transport also play a role. However, this does not apply to the OegRG. Although a disentanglement of the individual components based on aerial images and ALS data is not possible,[31] we characterized the frontal advance of the OegRG in several time steps between 1922 and 2021 by mapping the upper and lower front lines, calculating the volume change in the front and visually interpreting the DoDs. This revealed a distinct advance of the northern part of Front1 between 1922 and 1953. The reasons for this might be the warm phase between 1946 and 1951 (Figure 13), which increased permafrost temperature and therefore led to an enhanced internal plastic deformation of the permafrost ice.[3] Neither Front1 ($R^2 = -0.24$, $p = 0.86$) nor Front2 ($R^2 = 0.30$, $p = 0.20$) shows a significant relationship between mean surface elevation change in the front and mean annual air temperature. In addition to the aforementioned different components contributing to the front advance of a rock glacier, this could indicate that meltwater infiltration into the permafrost body from the glacier in the catchment and strong melt of superimposed dead ice, mentioned before, might have promoted deformation by reducing the effective stress in the permafrost ice[84] and promote basal sliding on the shear horizon by increasing pore water pressure.[4] Because these effects should have been more pronounced after the strong warming in the mid-1980s, but the frontal advance did not behave similarly, bedrock topography is very likely to play a key factor. Therefore, we suspect that the strong frontal advance of the lateral part of Front1 between 1922 and 1953 was caused by a combination of the previously mentioned factors with the overflow of the bedrock step, detected by Hausmann

et al.,[56] and a compressive flow along the lateral topographic constriction.

Further, we analyzed the front advance in combination with the horizontal surface flow velocities above the front, as this allowed us to draw conclusions about the frontal advance mechanisms of the two rock glacier lobes. Front1 showed hardly any advance of the lower front, except for the already-mentioned lateral frontal part, whereas the mean flow velocity above the front varied between 0.88 m/year (1953–1970) and 1.18 m/year (2012–2017). This indicates a very shallow layer of creeping material and/or very ice-rich sediments in Front1.[31,82] The fact that the volume balance of Front1 increased steadily, especially from 2012 onward, whereas the flow velocity in the area of the front decreased between 2012–2017 and 2017–2021, might point to a decoupled development in flow velocities at depth and/or or changed ratio of advance to ice melt.

Front2 appears to have a different mechanism of frontal advance compared to Front1. The advance across the entire front was distinct and 40 m between 1922 and 2021. In addition, flow velocities at the front were evident, averaging between 0.93 m/year (2017–2021) and 1.32 m/year (2012–2017). This indicates a block movement of the front, with both the upper part and the base of the front creeping downslope. Therefore, Front2 seems to have a lower ice content and/or a less steep decrease in flow velocity from the surface to depth.[31,82] This could also be due to the much steeper bedrock topography in the area of Front2 compared to Front1. The decrease in the positive volume changes in contrast to Front1 and the decoupling from the surface flow velocities at the front could indicate an independent change in the velocities at depth or an increased melting of ice in the front.

4.4 | Development in flow velocities

The flow velocities during the entire investigation period (1938–2021) ranged between a few centimeters per year and a maximum of 1.77 m/year measured in 2012–2017. Thus, the magnitudes were well within the range of annual flow movements of other rock glaciers in the Alps, which range between a few centimeters per year and a few meters per year.[18] Apart from these, some studies show a destabilization of rock glaciers, which results in a landslide-like movement with displacement rates of up to several tens of meters per year (e.g., Marcer et al.,[12] Roer et al.,[85] and Vivero and Lambiel[86]). The acceleration in the period between 1997 and 2006 has also been demonstrated by several studies across the Alps.[8,25,29,30,37,87] This increase in flow velocities on a decadal timescale has been explained by increasing mean annual air (see Figure 13) and ground temperatures as well as mechanisms of heat conduction and meltwater advection.[18,29,46,84] The further course of flow velocities in the following time periods can be linked to annual measurements of flow velocities on a variety of rock glaciers.[88] A regression analysis showed that in the case of Lobe1 ($R^2 = 0.11$, $p = 0.25$) there is no significant correlation between mean flow velocity and mean MAAT in the individual time steps, whereas Lobe2 ($R^2 = 0.53$, $p < 0.05$) shows a significant

relationship. In addition to other factors, described later, that influence flow velocity, this may indicate a delayed response of Lobe1, in particular to increased temperatures. This phenomenon can be observed for both lobes in the time period 1953–1970 where increased flow velocities of the two rock glacier lobes might be explained by a delayed response to relatively high temperatures between 1946 and 1951 (Figure 13). This phenomenon has also been observed by other multi-decadal rock glacier studies in the European Alps.[9,27,87] This could also explain the increased flow velocities of Profile2 between 1938 and 1953, whereby the strength of the flow velocity, which was higher than that in all subsequent epochs, cannot be explained by the short warm phase alone, as the temperature increase was stronger from the mid-1980s and over a longer period. This, together with the fact that Lobe1 does not show a significant relationship between flow velocity and MAAT, suggests that the melting of the massive dead ice bodies and the glacier situated above both rock glacier lobes between 1922 and 1953 might have influenced the rock glacier kinematics due to increased water availability and surface deformation caused by ice melting of the dead ice bodies. This hypothesis is supported by the fact that seasonal investigation of flow velocities revealed higher flow velocities during the melting season, suggesting an influence of meltwater on flow velocities of the OegRG.[50]

To our knowledge, apart from the study by Scapozza et al.,[30] there are no studies of rock glacier flow velocities before 1953 using a similar method. This made it difficult to put the increased flow rates between 1938 and 1953 into perspective. On the Stabbio di Largario rock glacier in the southern Swiss Alps, no increased flow velocities were measured between 1910–1924 and 1924–1940 compared to 1940–1996.[30] However, a comparison was difficult due to the different methods and measurement periods.

5 | CONCLUSION

Because there are hardly any studies on the dynamics of rock glaciers before the first aerial photographs in the Alps, the aim of this study was to put historical data (measurements and maps) into value for the investigation of the OegRG. By evaluating the FW1922 and the historical flow velocity measurements by Pillewizer,[53] relating them to existing data between 1953 and 2017,[24] and extending this time series with another ALS data set from 2021, it was possible to analyze the evolution of the two lobes of the OegRG over almost a century and relate them to the changes in temperature development. However, most explanations of the development in the OegRG remain rather hypothetical, and it must be clearly stated that in the case of historical data many uncertainties and error variables cannot be sufficiently quantified.

The geomorphic evolution of the two lobes of the OegRG between 1922 and 2021 was characterized by both similar general trends and differences in their development. Because the external forcing for the two lobes was almost identical, the different

mechanisms of frontal advance and the variations in temporal development of flow velocities and volume change may be due to differences in internal structure, bedrock topography, or upslope connection to the glacier (presence and size of the glacier). In terms of the general trends, the study suggests that the warm phase between 1946 and 1951 may have favored the increased values in both flow velocity and volume change before 1953. However, considering the strong and long-lasting temperature increase since the 1980s, this cannot be the only factor that controlled this development. Additional drivers might be the glacier cover of the OegRG during LIA, glacier forefield connection of the rock glacier, and lateral constriction of Front1.

Because such a development before 1953 is most likely not representative for all active rock glaciers, we see the need to analyze the geomorphic development of further rock glaciers before the first aerial photographs were taken in the early 1950s. These analyses could be of particular interest on rock glaciers that show increased flow rates between 1950 and 1970, such as the Dösen rock glacier[87] or the Ritigraben rock glacier.[28] Such investigations could help us to understand how to interpret the current dynamics in relation to a changing external forcing. In addition, factors influencing the kinematics of rock glaciers, such as an intermittent glacier cover or the glacier forefield connection, could be better understood in this way. Methodologically, such studies could be similar to this study, although monoplotting on historical terrestrial imagery and photogrammetric analysis of historical overlapping image pairs also seem to be promising approaches. This shows how important it can be for current research to retrieve historical data (e.g., maps, images, and measurements) and put into value and simultaneously demonstrates the importance of data storage and accessibility for future generations.

CONFLICT OF INTEREST

The authors declare that they have no conflict of interest. The funders had no role in the design of the study; in the collection, analyses, or interpretation of data; in the writing of the manuscript; or in the decision to publish the results.

DATA AVAILABILITY STATEMENT

All data, including ALS data, will presumably be made available after completion of the SEHAG (Sensitivity of High Alpine Geosystems to Climate Change Since 1850) research project. The data on flow velocity, surface elevation change, and front advance can be obtained on request.

ORCID

Fabian Fleischer https://orcid.org/0000-0002-4989-2092
Florian Haas https://orcid.org/0000-0002-4874-2527

REFERENCES

1. Barsch D. *Rockglaciers: Indicators for the present and former Geoecology in High Mountain environments, springer series in physical environment*. Vol. 16. Berlin Heidelberg, Berlin, Heidelberg: Springer; 1996:331. doi:10.1007/978-3-642-80093-1
2. Berthling I. Beyond confusion: rock glaciers as cryo-conditioned landforms. *Geomorphology*. 2011;131(3-4):98-106. doi:10.1016/j.geomorph.2011.05.002
3. Haeberli W, Hallet B, Arenson L, et al. Permafrost creep and rock glacier dynamics. *Permafrost Periglac Process*. 2006;17(3):189-214. doi:10.1002/ppp.561
4. Buchli T, Kos A, Limpach P, Merz K, Zhou X, Springman SM. Kinematic investigations on the Furggwanghorn rock glacier, Switzerland. *Permafrost Periglac Process*. 2018;29(1):3-20. doi:10.1002/ppp.1968
5. Cicoira A, Beutel J, Faillettaz J, Vieli A. Water controls the seasonal rhythm of rock glacier flow. *Earth Planet Sci Lett*. 2019b;528:115844. doi:10.1016/j.epsl.2019.115844
6. Cicoira A, Marcer M, Gärtner-Roer I, Bodin X, Arenson LU, Vieli A. A general theory of rock glacier creep based on in-situ and remote sensing observations. *Permafrost Periglac Process*. 2020;29(1):21-153. doi:10.1002/ppp.2090
7. Gärtner-Roer I, Brunner N, Delaloye R, Haeberli W, Kääb A, Thee P. Glacier-permafrost relations in a high-mountain environment: 5 decades of kinematic monitoring at the Gruben site, Swiss Alps. *Cryosph Discuss*. 2021;30:1-30.
8. Kellerer-Pirklbauer A, Kaufmann V. Deglaciation and its impact on permafrost and rock glacier evolution: new insight from two adjacent cirques in Austria. *Sci Total Environ*. 2018;621:1397-1414. doi:10.1016/j.scitotenv.2017.10.087
9. Kenner R, Pruessner L, Beutel J, Limpach P, Phillips M. How rock glacier hydrology, deformation velocities and ground temperatures interact: examples from the Swiss Alps. *Permafrost Periglac Process*. 2020; 31(1):3-14. doi:10.1002/ppp.2023
10. Krainer K, Bressan D, Dietre B, et al. A 10,300-year-old permafrost core from the active rock glacier Lazaun, southern Ötztal Alps (South Tyrol, northern Italy). *Quatern Res*. 2015;83(2):324-335. doi:10.1016/j.yqres.2014.12.005
11. Kummert M, Bodin X, Braillard L, Delaloye R. Pluri-decadal evolution of rock glaciers surface velocity and its impact on sediment export rates towards high alpine torrents. *Earth Surf Process Landf*. 2021; 105(15):113-3227. doi:10.1002/esp.5231
12. Marcer M, Cicoira A, Cusicanqui D, et al. Rock glaciers throughout the French Alps accelerated and destabilised since 1990 as air temperatures increased. *Commun Earth Environ*. 2021;2(1):383. doi:10.1038/s43247-021-00150-6
13. Wagner T, Kainz S, Krainer K, Winkler G. Storage-discharge characteristics of an active rock glacier catchment in the Innere Ölgrube, Austrian Alps. *Hydrol Process*. 2021;35(5):e14210. doi:10.1002/hyp.14210
14. Rangecroft S, Harrison S, Anderson K. Rock glaciers as water Stores in the Bolivian Andes: an assessment of their hydrological importance.

Arct Antarct Alpine Res. 2015;47(1):89-98. doi:10.1657/AAAR0014-029
15. Schaffer N, MacDonell S, Réveillet M, Yáñez E, Valois R. Rock glaciers as a water resource in a changing climate in the semiarid Chilean Andes. *Reg Environ Change*. 2019;19(5):1263-1279. doi:10.1007/s10113-018-01459-3
16. Jones DB, Harrison S, Anderson K. Mountain glacier-to-rock glacier transition. *Global Planet Change*. 2019;181:102999. doi:10.1016/j.gloplacha.2019.102999
17. Knight J, Harrison S, Jones DB. Rock glaciers and the geomorphological evolution of deglacierizing mountains. *Geomorphology*. 2019;324: 14-24. doi:10.1016/j.geomorph.2018.09.020
18. Delaloye R, Lambiel C, Gärtner-Roer I. Overview of rock glacier kinematics research in the Swiss Alps. *Geogr Helv*. 2010;65(2):135-145. doi:10.5194/gh-65-135-2010
19. Delaloye R, Perruchoud E, Bodin X, et al. Recent interannual variations of rock glacier creep in the European Alps, 9th International Conference on Permafrost, Fairbanks, Alaska, 29 Juni 2008–3 Juli 2008; 2008:343-348. doi:10.5167/UZH-7031
20. Kenner R, Phillips M, Beutel J, et al. Factors controlling velocity variations at short-term, seasonal and multiyear time scales, Ritigraben rock glacier, Western Swiss Alps. *Permafrost Periglac Process*. 2017; 28(4):675-684. doi:10.1002/ppp.1953
21. Wirz V, Gruber S, Purves RS, et al. Short-term velocity variations at three rock glaciers and their relationship with meteorological conditions. *Earth Surf Dyn*. 2016;4(1):103-123. doi:10.5194/esurf-4-103-2016
22. Avian M, Kaufmann V, Lieb GK. Recent and Holocene dynamics of a rock glacier system: the example of Langtalkar (Central Alps, Austria). *Norsk Geografisk Tidsskrift - Norwegian Journal of Geography*. 2005; 59(2):149-156. doi:10.1080/00291950510020637
23. Dusik J-M, Leopold M, Heckmann T, et al. Influence of glacier advance on the development of the multipart Riffeltal rock glacier, central Austrian Alps. *Earth Surf Process Landf*. 2015;40(7):965-980. doi:10.1002/esp.3695
24. Fleischer F, Haas F, Piermattei L, et al. Multi-decadal (1953–2017) rock glacier kinematics analysed by high-resolution topographic data in the upper Kauertal, Austria. *The Cryosphere*. 2021;15(12):5345-5369. doi:10.5194/tc-15-5345-2021
25. Hartl L, Fischer A, Stocker-Waldhuber M, Abermann J. Recent speed-up of an alpine rock glacier: an updated chronology of the kinematics of outer hochebenkar rock glacier based on geodetic measurements. *Geogr Ann Ser B*. 2016;98(2):129-141. doi:10.1111/geoa.12127
26. Kaufmann V, Landstädter R. Mapping of the 3D surface motion field of Doesen rock glacier (Ankogel group, Austria) and its Spatiotemporal change (1954-1998) by means of digital photogrammetry. *Grazer Schriften der Geographie Und Raumforschung*. 2007;43: 137-144.
27. Kellerer-Pirklbauer A, Kaufmann V. About the relationship between rock glacier velocity and climate parameters in Central Austria. *Aust J Earth Sci*. 2012;105:94-112.
28. Lugon R, Stoffel M. Rock-glacier dynamics and magnitude–frequency relations of debris flows in a high-elevation watershed: Ritigraben, Swiss Alps. *Global Planet Change*. 2010;73(3-4):202-210. doi:10.1016/j.gloplacha.2010.06.004
29. Roer I. Rockglacier kinematics in a high mountain geosystem, Dissertation, Mathematisch-Naturwissenschaftliche Fakultät, Rheinische Friedrich-Wilhelms-Untiversität Bonn, Bonn; 2005: 263.
30. Scapozza C, Lambiel C, Bozzini C, Mari S, Conedera M. Assessing the rock glacier kinematics on three different timescales: a case study from the southern Swiss Alps. *Earth Surf Process Landf*. 2014;39(15): 2056-2069. doi:10.1002/esp.3599
31. Kääb A, Strozzi T, Bolch T, et al. Inventory and changes of rock glacier creep speeds in Ile Alatau and Kungöy ala-too, northern Tien Shan,

since the 1950s. *Cryosphere*. 2021;15(2):927-949. doi:10.5194/tc-15-927-2021

32. Vivero S, Bodin X, Farías-Barahona D, et al. Combination of aerial, satellite, and UAV photogrammetry for quantifying rock glacier kinematics in the dry Andes of Chile (30°S) since the 1950s. *Front Remote Sens*. 2021;2:117. doi:10.3389/frsen.2021.784015

33. Janke JR. Photogrammetric analysis of front range rock glacier flow rates. *Geogr Ann Ser B*. 2005;87(4):515-526. doi:10.1111/j.0435-3676.2005.00275.x

34. Tanarro LM, Palacios D, Andrés N, et al. Unchanged surface morphology in debris-covered glaciers and rock glaciers in Tröllaskagi peninsula (northern Iceland). *Sci Total Environ*. 2019;648:218-235. doi:10.1016/j.scitotenv.2018.07.460

35. Wangensteen B, Guðmundsson Á, Eiken T, Kääb A, Farbrot H, Etzelmüller B. Surface displacements and surface age estimates for creeping slope landforms in northern and eastern Iceland using digital photogrammetry. *Geomorphology*. 2006;80(1-2):59-79. doi:10.1016/j.geomorph.2006.01.034

36. Bodin X, Thibert E, Fabre D, et al. Two decades of responses (1986-2006) to climate by the Laurichard rock glacier, French Alps. *Permafrost Periglac Process*. 2009;20(4):331-344. doi:10.1002/ppp.665

37. Kaufmann V, Seier G, Sulzer W, et al. Rock glacier monitoring using aerial photographs: conventional vs. UAV-based mapping - a comparative study. *Int Arch Photogramm Remote Sens Spatial Inf Sci*. 2018; XLII-1:239-246. doi:10.5194/isprs-archives-XLII-1-239-2018

38. Monnier S, Kinnard C. Pluri-decadal (1955–2014) evolution of glacier-rock glacier transitional landforms in the Central Andes of Chile (30–33°S). *Earth Surf Dyn*. 2017;5:493-509. doi:10.5194/esurf-5-493-2017

39. Capt M, Bosson J-B, Fischer M, Micheletti N, Lambiel C. Decadal evolution of a very small heavily debris-covered glacier in an Alpine permafrost environment. *J Glaciol*. 2016;62(233):535-551. doi:10.1017/jog.2016.56

40. Mertes JR, Gulley JD, Benn DI, Thompson SS, Nicholson LI. Using structure-from-motion to create glacier DEMs and orthoimagery from historical terrestrial and oblique aerial imagery. *Earth Surf Process Landf*. 2017;42(14):2350-2364. doi:10.1002/esp.4188

41. Midgley NG, Tonkin TN. Reconstruction of former glacier surface topography from archive oblique aerial images. *Geomorphology*. 2017; 282:18-26. doi:10.1016/j.geomorph.2017.01.008

42. Mölg N, Bolch T. Structure-from-motion using historical aerial images to analyse changes in glacier surface elevation. *Remote Sens (Basel)*. 2017;9:1021. doi:10.3390/rs9101021

43. Vargo LJ, Anderson BM, Horgan HJ, Mackintosh AN, Lorrey AM, Thornton M. Using structure from motion photogrammetry to measure past glacier changes from historic aerial photographs. *J Glaciol*. 2017;63(242):1105-1118. doi:10.1017/jog.2017.79

44. Böhlert R. A combination of relative-numerical dating methods indicates two high Alpine rock glacier activity phases after the glacier advance of the younger Dryas. *Open Geogr J*. 2011;4(1):115-130. doi:10.2174/1874923201104010115

45. Scapozza C, Del Siro C, Lambiel C, Ambrosi C. Schmidt hammer exposure-age dating of periglacial and glacial landforms in the southern Swiss Alps based on R-value calibration using historical data. *Geogr Helv*. 2021;76(4):401-423. doi:10.5194/gh-76-401-2021

46. Kääb A, Frauenfelder R, Roer I. On the response of rockglacier creep to surface temperature increase. *Global Planet Change*. 2007;56(1-2):172-187. doi:10.1016/j.gloplacha.2006.07.005

47. Müller J, Vieli A, Gärtner-Roer I. Rock glaciers on the run - understanding rock glacier landform evolution and recent changes from numerical flow modeling. *The Cryosphere*. 2016;10(6):2865-2886. doi:10.5194/tc-10-2865-2016

48. Cicoira A, Beutel J, Faillettaz J, Gärtner-Roer I, Vieli A. Resolving the influence of temperature forcing through heat conduction on rock

glacier dynamics: a numerical modelling approach. *The Cryosphere*. 2019a;13(3):927-942. doi:10.5194/tc-13-927-2019

49. Jansen F, Hergarten S. Rock glacier dynamics: stick-slip motion coupled to hydrology. *Geophys Res Lett*. 2006;33(10). doi:10.1029/2006GL026134

50. Krainer K, Mostler W. Flow velocities of active rock glaciers in the Austrian Alps, Geografiska Annaler: series a. *Phys Geogr*. 2006;88 A(4):267-280. doi:10.1111/j.0435-3676.2006.00300.x

51. Brunetti M, Lentini G, Maugeri M, et al. Climate variability and change in the greater Alpine region over the last two centuries based on multi-variable analysis. *Int J Climatol*. 2009;29(15):2197-2225. doi:10.1002/joc.1857

52. Finsterwalder S. Begleitworte zur Karte des Gepatschferners. *Zeitschrift für Gletscherkunde*. 1928;XVI:20-41.

53. Pillewizer W. Untersuchungen an Blockstromen der Otztaler Alpen, Abhandlungen des Geographischen Instituts der Freien Universität Berlin, Band 5, 37–50, available at: https://e-docs.geo-leo.de/bitstream/handle/11858/7701/agi_fels_schultze_1957.pdf?sequence=1&isallowed=y#page=37, 1957.

54. Fliri F. Das Klima der Alpen im Raume von Tirol, Monographien zur Landeskunde Tirol, Folge 1, Universitätsverlag, Innsbruck; 1975: 454.

55. Berger J, Krainer K, Mostler W. Dynamics of an active rock glacier (Ötztal Alps, Austria). *Quatern Res*. 2004;62(3):233-242. doi:10.1016/j.yqres.2004.07.002

56. Hausmann H, Krainer K, Brückl E, Ullrich C. Internal structure, ice content and dynamics of Ölgrube and Kaiserberg rock glaciers (Ötztal Alps, Austria) determined from geophysical surveys. *Aust J Earth Sci*. 2012;105:12-31.

57. Groh T, Blöthe JH. Rock glacier kinematics in the Kaunertal, Ötztal Alps, Austria. *Geosciences*. 2019;9(9):373. doi:10.3390/geosciences9090373

58. Scambos T, Dutkiewicz M, Wilson J, Bindschadler R. Application of image cross-correlation to the measurement of glacier velocity using satellite image data. *Remote Sens Environ*. 1992;42(3):177-186. doi:10.1016/0034-4257(92)90101-O

59. Fey C, Krainer K. Analyses of UAV and GNSS based flow velocity variations of the rock glacier Lazaun (Ötztal Alps, South Tyrol, Italy). *Geomorphology*. 2020;365:107261. doi:10.1016/j.geomorph.2020.107261

60. Besl PJ, McKay ND. A method for registration of 3-D shapes. *IEEE Trans Pattern Anal Mach Intell*. 1992;14(2):239-256. doi:10.1109/34.121791

61. Hutchinson M, Xu T, Stein J. Recent Progress in the ANUDEM Elevation Gridding Procedure, in: Geomorphometry 2011, Redlands, California, USA; 2011:19-22.

62. Freudiger D, Mennekes D, Seibert J, Weiler M. Historical glacier outlines from digitized topographic maps of the Swiss Alps. *Earth Syst Sci Data*. 2018;10(2):805-814. doi:10.5194/essd-10-805-2018

63. McNabb R. pybob, available at: https://github.com/iamdonovan/pybob/tree/44467f670811548c4cabaa5c29eb4b6a66615a6d, 2019.

64. Nuth C, Kääb A. Co-registration and bias corrections of satellite elevation data sets for quantifying glacier thickness change. *Cryosphere*. 2011;5(1):271-290. doi:10.5194/tc-5-271-2011

65. Anderson SW. Uncertainty in quantitative analyses of topographic change: error propagation and the role of thresholding. *Earth Surf Process Landf*. 2019;44(5):1015-1033. doi:10.1002/esp.4551

66. Lane SN, Westaway RM, Murray Hicks D. Estimation of erosion and deposition volumes in a large, gravel-bed, braided river using synoptic remote sensing. *Earth Surf Process Landf*. 2003;28(3):249-271. doi:10.1002/esp.483

67. Abermann J, Fischer A, Lambrecht A, Geist T. On the potential of very high-resolution repeat DEMs in glacial and periglacial environments. *Cryosphere*. 2010;4(1):53-65. doi:10.5194/tc-4-53-2010

68. Klug C, Bollmann E, Galos SP, et al. Geodetic reanalysis of annual gla-ciological mass balances (2001–2011) of Hintereisferner, Austria. *Cryosphere*. 2018;12(3):833-849. doi:10.5194/tc-12-833-2018

69. Fischer A, Schwaizer G, Seiser B, Helfricht K, Stocker-Waldhuber M. High-resolution inventory to capture glacier disintegration in the Austrian Silvretta. *The Cryosphere*. 2021;15(10):4637-4654. doi:10.5194/tc-15-4637-2021

70. Rastner P, Joerg PC, Huss M, Zemp M. Historical analysis and visuali-zation of the retreat of Findelengletscher, Switzerland, 1859–2010. *Global Planet Change*. 2016;145:67-77. doi:10.1016/j.gloplacha.2016.07.005

71. Salerno F, Buraschi E, Bruccoleri G, Tartari G, Smiraglia C. Glacier surface-area changes in Sagarmatha national park, Nepal, in the second half of the 20th century, by comparison of historical maps. *J Glaciol*. 2008;54(187):738-752. doi:10.3189/002214308786570926

72. Scheidl C, Rickenmann D, Chiari M. The use of airborne LiDAR data for the analysis of debris flow events in Switzerland. *Nat Hazards Earth Syst Sci*. 2008;8(5):1113-1127. doi:10.5194/nhess-8-1113-2008

73. Müller J, Gärtner-Roer I, Thee P, Ginzler C. Accuracy assessment of airborne photogrammetrically derived high-resolution digital eleva-tion models in a high mountain environment. *ISPRS J Photogr Remote Sens*. 2014;98:58-69. doi:10.1016/j.isprsjprs.2014.09.015

74. Betz-Nutz S. Vergleichende photogrammetrische Untersuchungen zu langfristigen Veränderungen der Morphodynamik auf neuzeitlichen Lateralmoränen ausgewählter Alpengletscher, Universitätsbibliothek Eichstätt-Ingolstadt; 2021.

75. RGIK. Towards standard guidelines for inventorying rock glaciers: practical concepts (version 2.0), IPA Action Group Rock glacier inven-tories and kinematics. https://bigweb.unifr.ch/Science/Geosciences/Geomorphology/Pub/Website/IPA/CurrentVersion/Current_Practical_Concepts_Inventorying_Rock_Glaciers.pdf, last access: 2 August 2022, 2022.

76. Janke JR. Using airborne LiDAR and USGS DEM data for assessing rock glaciers and glaciers. *Geomorphology*. 2013;195:118-130. doi:10.1016/j.geomorph.2013.04.036

77. Anderson RS, Anderson LS, Armstrong WH, Rossi MW, Crump SE. Glaciation of alpine valleys: the glacier – debris-covered glacier – rock glacier continuum. *Geomorphology*. 2018;311:127-142. doi:10.1016/j.geomorph.2018.03.015

78. Deline P. Change in surface debris cover on Mont Blanc massif gla-ciers afer the 'Little ice Age' termination. *The Holocene*. 2005;15(2):302-309. doi:10.1191/0959683605hl809rr

79. Lugon R, Delaloye R, Serrano E, Reynard E, Lambiel C, González-Trueba JJ. Permafrost and little ice age glacier relationships, Posets massif, Central Pyrenees, Spain. *Permafrost Periglac Process*. 2004;15(3):207-220. doi:10.1002/ppp.494

80. Ribolini A, Chelli A, Guglielmin M, Pappalardo M. Relationships between glacier and rock glacier in the maritime Alps, Schiantala Val-ley, Italy. *Quatern Res*. 2007;68(3):353-363. doi:10.1016/j.yqres.2007.08.004

81. Haberkorn A, Kenner R, Noetzli J, Phillips M. Changes in ground tem-perature and dynamics in mountain permafrost in the Swiss Alps. *Front Earth Sci*. 2021;9:35. doi:10.3389/feart.2021.626686

82. Kääb A, Reichmuth T. Advance mechanisms of rock glaciers. *Permafrost Periglac Process*. 2005;16(2):187-193. doi:10.1002/ppp.507

83. Kummert M, Delaloye R. Mapping and quantifying sediment transfer between the front of rapidly moving rock glaciers and torrential gullies. *Geomorphology*. 2018;309:60-76. doi:10.1016/j.geomorph.2018.02.021

84. Ikeda A, Matsuoka N, Kääb A. Fast deformation of perennially frozen debris in a warm rock glacier in the Swiss Alps: an effect of liq-uid water. *J Geophys Res*. 2008;113(F1):212. doi:10.1029/2007JF000859

85. Roer I, Haeberli W, Avian M, et al. Observations and considerations on destabilizing active rock glaciers in the European Alps, 9th interna-tional conference on permafrost, Fairbanks, Alaska, 29 June 2008-03 July 2008; 2008:1505-1510.

86. Vivero S, Lambiel C. Monitoring the crisis of a rock glacier with repeated UAV surveys. *Geogr Helv*. 2019;74(1):59-69. doi:10.5194/gh-74-59-2019

87. Kellerer-Pirklbauer A, Lieb GK, Kaufmann V. The Dösen rock glacier in Central Austria: a key site for multidisciplinary long-term rock gla-cier monitoring in the eastern Alps. *AJES*. 2018;110(2). doi:10.17738/ajes.2017.0013

88. PERMOS. 2021, Swiss permafrost bulletin 2019/2020, 2021, Noetzli, J. and Pellet, C. (eds.); 2021:21. doi:10.13093/permos-2021